Metadata of the chapter that will be visualized online

Chapter Title	Nanopore-Penetration Sensing Effects for Target DNA Sequencing via Impedance Difference Between Organometallic-Complex-Decorated Carbon Nanotubes with Twisted Single-Stranded or Double-Stranded DNA	
Copyright Year	2020	
Copyright Holder	Springer Nature B.V.	
Author	Family Name	**Babenko**
	Particle	
	Given Name	**A. S.**
	Suffix	
	Division	Bioorganics Department
	Organization	Belarusian State Medical University
	Address	Minsk, Belarus
Corresponding Author	Family Name	**Grushevskaya**
	Particle	
	Given Name	**H. V.**
	Suffix	
	Division	Physics Department
	Organization	Belarusian State University
	Address	Minsk, Belarus
	Email	grushevskaja@bsu.by
Author	Family Name	**Krylova**
	Particle	
	Given Name	**N. G.**
	Suffix	
	Division	Physics Department
	Organization	Belarusian State University
	Address	Minsk, Belarus
	Email	nina-kr@tut.by
Author	Family Name	**Lipnevich**
	Particle	
	Given Name	**I. V.**
	Suffix	
	Division	Physics Department
	Organization	Belarusian State University
	Address	Minsk, Belarus
	Email	lipnevich@bsu.by

Author	Family Name	**Egorova**
	Particle	
	Given Name	**V. P.**
	Suffix	
	Organization	Belarusian State Pedagogical University
	Address	Minsk, Belarus
Author	Family Name	**Chakukov**
	Particle	
	Given Name	**R. F.**
	Suffix	

Abstract	We offer a highly sensitive and reproducible dielectric-spectroscopy assay of deoxyribonucleic acid (DNA) sequence on a platform of quantum graphene-like structures arranged on nanoporous alumina to correctly identifying an infectious agent in a native double-stranded (ds) DNA. The hybridization of complementary target DNA with probe DNA in the sensor sensitive layer leads to penetration of the formed single-stranded (ss) target DNA into the underlayer nanoporous anodic alumina through the nanocavities of LB-film from organometallic complexes. This results in linking of MWCNT ends, shielding of Helmholtz double layer and following decrease of electrical capacitance of the sensor. The novel electrochemical impedimetric DNA sensor with self-organized multi-walled carbon nanotube (MWCNT) bundles decorated by organometallic complexes as transducer has been utilized to detect the viral DNA in the biological samples of patients with virus infection at DNA concentration as low as 1.0–1.3 ng/μL.

Keywords (separated by "-")	Multi-walled carbon nanotube (MWCNT) - Nanopore-penetration sensing effect - Double-stranded DNA - Single-stranded DNA

Chapter 17
Nanopore-Penetration Sensing Effects for Target DNA Sequencing via Impedance Difference Between Organometallic-Complex-Decorated Carbon Nanotubes with Twisted Single-Stranded or Double-Stranded DNA

A. S. Babenko, H. V. Grushevskaya, N. G. Krylova, I. V. Lipnevich, V. P. Egorova, and R. F. Chakukov

Abstract We offer a highly sensitive and reproducible dielectric-spectroscopy assay of deoxyribonucleic acid (DNA) sequence on a platform of quantum graphene-like structures arranged on nanoporous alumina to correctly identifying an infectious agent in a native double-stranded (ds) DNA. The hybridization of complementary target DNA with probe DNA in the sensor sensitive layer leads to penetration of the formed single-stranded (ss) target DNA into the underlayer nanoporous anodic alumina through the nanocavities of LB-film from organometallic complexes. This results in linking of MWCNT ends, shielding of Helmholtz double layer and following decrease of electrical capacitance of the sensor. The novel electrochemical impedimetric DNA sensor with self-organized multi-walled carbon nanotube (MWCNT) bundles decorated by organometallic complexes as transducer has been utilized to detect the viral DNA in the biological samples of patients with virus infection at DNA concentration as low as 1.0–1.3 ng/μL.

A. S. Babenko
Bioorganics Department, Belarusian State Medical University, Minsk, Belarus

H. V. Grushevskaya (✉) · N. G. Krylova · I. V. Lipnevich · R. F. Chakukov
Physics Department, Belarusian State University, Minsk, Belarus
e-mail: grushevskaja@bsu.by; nina-kr@tut.by; lipnevich@bsu.by

V. P. Egorova
Belarusian State Pedagogical University, Minsk, Belarus

J. Bonča, S. Kruchinin (eds.), *Advanced Nanomaterials for Detection of CBRN*,
NATO Science for Peace and Security Series A: Chemistry and Biology,
https://doi.org/10.1007/978-94-024-2030-2_17

Keywords Multi-walled carbon nanotube (MWCNT) · Nanopore-penetration sensing effect · Double-stranded DNA · Single-stranded DNA

17.1 Introduction

Advances in molecular biology in recent decades are connected with utilizing third-generation DNA-nanosequencing label-free methods [1]. But, the sensitivity of these methods appears to be not enough to recognize a viral infection at the stage of fewness lesions of body cells (so called the window period, or the serologic window). In addition the modern DNA-sequencing methods take quite a lot of time for target viral genome identification. Human parvovirus infection leads to the serious complications, including transient aplastic crisis, chronic anemia, and fetal death. In such cases effectiveness of the infectious diseases treatment often depends on the correct identifying an infectious agent, namely on the performance of medical diagnostic methods. High-sensitive methods to detect viral infection is challenge.

To reveal human parvovirus infection for medical practice we offer a dielectric spectroscopy method based on highly selective hybridization interactions of noncovalent complementary single-stranded ss-DNA molecules. Interacting probe ss-DNA and target genomic linear ss-DNA of samples under investigation form a ds-DNA helix of homoduplex on sensor surface for detection of parvovirus infection. The novel high-sensitive method reliably detects the presence or absence of parvovirus in a sample and does not demand expensive consumable materials.

The goal of the paper is to study effects of penetration of DNA in nanopores at electrochemical DNA sensing on organometallic-complex-decorated MWCNTs deposited on a nanoporous surface. We will utilize the novel label-free electrochemical DNA-nanosensor based on carbon nanotubes (CNTs) to identify viral status of native genomic DNA via impedance difference between the metal-decorated MWCNTs with twisted ss- or ds-DNA.

17.2 Materials and Methods

17.2.1 Reagents

We utilized two types of ss-DNA probes to recognize parvovirus sequences: direct primer sequence to $3' \rightarrow 5'$–ss-DNA-chain and revers one to $5' \rightarrow 3'$–ss-DNA-chain. The direct and revers primers are denoted through $B19VF4$ and $B19VR4$, respectively. The ds-DNA samples have been obtained from blood serum of patients with parvovirus infection (DNA_{pvi}, $i = 1, 2, 3$) and of practically healthy donors (DNA_{hi}, $i = 1, 2, 3$) as negative control. Spectrophotometric data for the infection DNA samples are presented in Table 17.1. The spectrofluorimetric method was used

Table 17.1 Optical densities OD_λ and their differences for different wavelengthes λ and concentration C for parvovirus infection DNA samples

Type of sample	$(OD_{260} - OD_{320})/(OD_{280} - OD_{320})$	OD_{320}	C, μg/mL
DNA_{pv1}	1.8	0.05	4.5
DNA_{pv2}	1.9	0.23	3.8

also to measure the concentration of DNA_{hi}, $i = 1, 2, 3$. The concentration of DNA was estimated about 4.5–5.0 ng/μL.

To calibrate a label-free sequencing an oncogene KRAS, native DNA isolated from colon-cancer tumor, and placental DNA were utilized as a marker gene. The tumor tissue of patients with established diagnosis of colon cancer carrying a mutation single nucleotide polymorphism (SNP) in the second KRAS-exon, codon 12, GGT>GAT were used. Probe DNA $KRAS_m$ is a label-free probe oligonucleotide sequence for the KRAS-gene with SNP. RNA and proteins contents in high-purity ds-DNA (1.03 mg/ml in 10^{-5} M Na_2CO_3 buffer medium) isolated from placenta tissue of healthy donors were less that 0.1% (optical density ratio $D_{260}/D_{230} = 2.378$ and $D_{260}/D_{280} = 1.866$, respectively).

All DNA probes were purchased in "Primetech ALC" (Minsk, Belarus). Length of the oligonucleotides does not exceed 20 nucleotides.

To construct an electrochemical transducer MWCNTs are selected from MWCNTs with diameters ranging from 2.0 to 5 nm and length of ~2.5 μm. The original MWCNTs and single walled CNTs (SWCNTs) were obtained by the method of chemical vapor deposition (CVD-method) [2]. MWCNTs were covalently modified by carboxyl groups and non-covalently functionalized by stearic acid molecules. Salts $Fe(NO_3)_3 \cdot 9H_2O$, $Ce_2(SO_4)_3$ (Sigma, USA), hydrochloric acid, deionized water were used to preparate subphases. Iron-containing films were fabricated from an amphiphilic oligomer of thiophene derivatives with chemically bounded hydrophobic 16-link hydrocarbon chain: 3-hexadecyl-2,5-di(thiophen-2-yl)-1H-pyrrole (H-DTP, H-dithionilepyrrole). H-dithionilepyrrole was synthesized by a method proposed in [3]. Working solution of H-dithionilepyrrole, 1.0 mM, was prepared by dissolving precisely weighted substances in hexane. All salt solutions have been prepared with deionized water with resistivity 18.2 MΩ·cm.

All used materials belong to class of analytical pure reagents.

17.2.2 Methods

Impedance Measurements. Electro-physical studies have been performed using planar interdigital electrode structures on pyroceramics support. N pairs, $N = 20$ of aluminum electrodes are arranged in an Archimedes-type spiral configuration. Every such pair is an "open type" capacitor. The dielectric coating of the electrodes represents itself a nanoporous anodic alumina layer (AOA) with a pore diameter of 10 nm. To excite harmonic auto-oscillations of electric current

(charging-discharging processes in the capacitors), the sensor was connected as the capacitance C into the relaxation resistance (R) – capacitor (C) oscillator (self-excited RC-oscillator) [1, 4]. Operating of such RC-generator is based on the principle of self-excitation of an amplifier with a positive feedback on the quasi-resonance frequency. The capacitance C of the sensor entered in measuring RC-oscillating circuit has been calculated by the formula $C = 1/(2\pi Rf)$, where R is the measuring resistance, f is the frequency of quasi-resonance.

Biosensitive nanostructured layers which transduce hybridization signals have been fabricated by Langmuir–Blodgett (LB) technique. The biosensitive coating consists of five monomolecular LB-layers (LB-monolayers) fabricated from nanocyclic complexes of high-spin octahedral iron with dithionylpyrrole (DTP) ligands [5]. Complexes of carboxylated hydrophilic MWCNT with different DNA-probes have been deposited on the LB-film of metal-containing conducting dithionylpyrrole polymer [4]. The synthesized LB-nanoheterostructures were suspended on the interdigital electrode system. The fabricated capacitive DNA-nanosensors are sensors of non-Faraday type.

The response to the interactions between the DNA samples and the viral DNA probes has been detected on nanosensors F14, F24, F32 with the direct primers as DNA probes and on the nanosensors R0, R4, R18 with the revers primers as DNA probes. A DNA-nanosensor K11 with the mutant DNA probe $KRAS_m$ recognized SNP in the DNA samples of colon cancer tissue. All electrochemical measurements are performed in deionized water.

All results were confirmed by the method of sequencing by Sanger. We have discriminated mutation and wild type in 100% of 20 samples.

Langmuir–Blodgett technique. A fabrication of the LB-monolayers was carried out on an automated hand-made Langmuir trough with controlled deposition on a substrate, and with computer user interface working under Microsoft Windows operational system. Control of the surface tension has been performed by a highly sensitive resonant inductive sensor. The Y-type transposition of monolayers on supports was performed by their vertical dipping. The complexes $Fe(II)DTP_3$ of high-spin Fe(II) with DTP ligands were synthesized by LB-method at compression of H-dithionilepyrrole molecules on the surface of subphase with salts of three-valence Fe [5]. Horizontally and vertically arranged LB-MWCNT-bundles can be fabricated from the carboxylated multi-walled CNTs [6–11].

We use the LB-technique to deposit two LB-monolayers of stearic acid micelles with DNA/MWCNT complexes inside on five-monolayer LB-film of the organometallic Ce-containing Fe(II)DTP-complexes.

Fabrication of micellar DNA/MWCNT complexes. The micellar complexes ds-DNA/MWCNT and oligonucleotide/MWCNT were obtained by means of ultrasonic treatment of alcoholic solution of ds-DNA or oligonucleotide with MWCNT [6]. Then, the complexes were mixed with a solution of stearic acid in deionized water or in hexane. The resulting mixtures were homogenized by ultrasonic treatment to form hydrophilic or hydrophobic (reverse) micelles of stearic acid with complexes ds-DNA/MWCNT or oligonucleotide/MWCNT inside them [12].

Raman spectroscopy studies. Spectral studies in visible range were carried out using a confocal micro-Raman spectrometer Nanofinder HE ("LOTIS-TII", Tokyo, Japan–Belarus) by laser excitation at wavelengths 355, 473 and 532 nm with power in range from 0.0001 to 20 mW at room (RT) and low temperatures.

17.3 Results

17.3.1 Transducer Characterization

A transducer of electrochemical DNA-sensor is a layered nanoheterostructure consisting of two LB-monolayers of complexes MWCNT/DNA-probe which are deposited on five LB-monolayer of nanocyclic complexes of octahedral high-spin Fe(II) with the dithionilepyrrole ligands. Pyrrole rings of conducting polymer are able to reversible oxidation and reduction [13]. Cation-active (cationic) oxidized pyrrole rings holds dsDNA molecules fixed [14]. This self-redox activity provides DNA fixation during enough time for complementary hybridization, electrostatic repulsion of non-specific-bounded target DNA molecules and leaving from sensor surface in the phase of pyrrole reduction.

Characteristic frequencies of Raman light scattering for the CNTs, DNA, complexes DNA/MWCNT, and MWCNT-bundles arranged in stearic-acid micelles and thin LB-films are presented in Tables 17.2, 17.3, and 17.4. Comparison of Raman spectra of SWCNTs, original MWCNTs, and micellar MWCNTs shown in Table 17.2 demonstrates that the sensitive layer contains CNTs with some number of walls (about two walls). MWCNTs, which has been selected for transducer, practically do not contain impurities, as characteristic vibration mode D are absent in Raman spectrum of micellar MWCNTs. Since a part of MWCNT charge carriers is localized on the support defects the peak D appears in the Raman spectrum of LB-MWCNT-film at laser excitation with wavelength $\lambda = 532$ nm (see Table 17.2). However, decreasing in amplitude the peak D shifts to low frequencies at laser excitation with wavelength $\lambda = 355$ nm (Table 17.2). It testifies that the charge carriers confined on the MWCNT surface a can not participate in charge transport onto high-excited impurity levels. Presence of them on the lower excited impurity DNA-levels due $\pi - \pi$-interactions quenches light scattering with wave length $\lambda = 532$ nm in both ds-DNA and oligonucleotides (Tables 17.3 and 17.4).

Quinone can direct interact with DNA by forming covalently bonds with DNA bases as menadione, p-benzoquinone and mitomycin C [23–25] or by intercalating into DNA helix as anthracyclines [26]. Quinones can also interact with CNTs due to $\pi - \pi$ stacking onto the polyaromatic surface of nanotubes [27]. We utilized such a quinone as thymoquinone to prove the presence of recognized complementary target ss-DNA in the senor covering. According data in Fig. 17.1a, thymoquinone interacts with MWCNTs functionalized by DNA because decrease in the sensor capacity occurs at addition of thymoquinone at concentrations 1–50 μmol/L. Since the

Table 17.2 Characteristic molecular vibrations, observed in the Raman spectra of different samples with CNTs at RT, laser excitation with different wavelengths λ

Sample	Bands, cm^{-1}	Assignment or vibration peaks of similar molecular groups, cm^{-1}; λ
Dry SWCNTs*	179(RBM), 1343(D), 1592(G), 2444(D″ + D), 2680(2D), 2930(D″D), 3184(2G).	λ = 532 nm
	176.6(RBM), 1352(D), 1567, 1591(G), 2446 (D″ + D), 2704(2D), 2930(D″D), 3182(2G)	λ = 473 nm
Dry MWCNTs	1328(D), 1566(G), 2450 (D″ + D), 2660(2D), 2890 (D′ + D)	[15]; λ = 532 nm
SA micelles	1064.5, 1180, 1298.6, 1440.2, 1459.3, 2847, 2882	Pure SA: 863.2, 885.3, 1065.8, 1079.1, 1121.4, 1180.5, 1299.0, 1422.9, 1440, 1459, 1664.6, 2852.4, 2873.9, 2898.3, 2925.4 [16, 17]; λ = 532 nm
MWCNTs inside SA-micelles	163(RBM), 1575(G), 2430(D″ + D), 2648(2D), 3152(2G)	CNT with diameter 2–2.5 nm, pick *D* is practically absent [18]; λ = 532 nm
Thin LB-film from MWCNTs and SA	1350(D), 1573(G), 2406.68(D″ + D), 2683(2D), 2923(D′ + D).	Two LB-monolayers; λ = 473 nm
	1403(D), 1586(G), 2450 (D″ + D), 2810(2D), 2983(D′ + D)	Three LB-monolayers; λ = 355 nm

*Vibration modes of CNT are labeled in the following way. RBM is a radial breathing mode; peaks D, 2D, D′ + D, D″ + D, and D″D are vibrations near $K(K')$-point in a graphene Brillouin zone; peaks G, 2G are vibrations near Γ-point in the zone

MWCNTs are covered by a dense layer of the ss-DNA probe $KRAS_m$ this screening testifies that the quinone penetrates into DNA/MWCNT complexes. Hence, the homoduplexes between $KRAS_m$ and complementary target ss-DNA of colon cancer tumor with SNP are formed on the sensor surface K11.

17.3.2 *Electrochemical Impedance Spectroscopy Analysis*

The DNA-nanosensors were placed into deionized water. An electrical double (Helmholtz) layer is formed on the interface. Typical frequency dependencies of the sensor capacity are presented in Fig. 17.1b, c. The principe of target DNA sequence detection is based on shielding near-electrode Helmholtz layer that leads to decrease electric capacitance of double layer in a case of complementary target

Table 17.3 Characteristic molecular vibrations, observed in the Raman spectra of native DNA and complexes native DNA/MWCNT at different temperatures T, laser excitation with different wavelengths λ

Sample	Bands, cm^{-1}	Assignment or vibration peaks of similar molecular groups, cm^{-1}; λ; T
Dry placental DNA*	663.6(T,G,A), 728.2(A), 783(C), 802, 881.6, 963.6, 1014(d), 1060.64(d(CO)), 1100(DP), 1141.25, 1181.3(T,C), 1208.9, 1245.67(T), 1303.53(A), 1334(A), 1373.1(T,A,Gu), 1418.2(T,d(CH2)), 1442, 1460(d(CH2)), 1484(A,Gu), 1504.8(A), 1528.6(C), 1573(A,T), 1661(T,Gu(C=O)), 2747(d(CH)), 2894(d(CH)), 2955.36(d(CH))	DNA in A-form DNA; λ = 473 nm, RT
Dry calf DNA	663(T,G,A), 682(G), 727(A), 743(T,d), 783(C), 1012(d), 1060(d(CO)), 1100 (DP), 1181(T,C), 1243(T), 1308(A), 1335(A), 1372(T,A,Gu), 1418(T, d(CH2)), 1460(d(CH2)), 1484(A,Gu), 1508(A), 1528(C), 1574(A,T), 1664(T,Gu(C=O)), 2894(d(CH)), 2950(d(CH)), 2957(d(CH))	DNA in A-form [19, 20]
Placental DNA inside SA-micelles	835, 880, 920, 1020, 1050(d(CO)), 1100(DP), 1140, 1185(T,C), 1245(T), 1270(C,A), 1300(A), 1340(A), 1370(Gu,T,A), 1420(A,Gu), 1438(Gu), 1480(A,C), 1490(A,Gu), 1520(A), 1580(Gu,A), 1607(A), 1641(Gu,T), 2721(d(CH)), 2845.6, 2880.7(d(CH)), 2921(d(CH))	Deprotonated DNA at RT; λ = 532 nm. 1605 and 1609 are the characteristic vibrations of the group C=N in adenine of DNA and of the group NH_2 of ds-DNA [12, 18, 21, 22]; 2845.6 is the characteristic frequency of stearic acid
Placental-DNA-encased MWCNTs inside SA-micelles	1343(D), 1573(G), 2460(D″ + D), 2686(2D), 2930(D′ + D) 1358(D), 1582(G), 2446(D″ + D), 2710(2D), 2927(D′ + D) 1400(D), 1581(G), 2361(D″ + D), 2810(2D), 2970(D′ + D) 1350(D), 1587(G), 2467(D″ + D), 2698(2D), 1091.1(DP), 1124.5, 1175(T,C), 1621(Gu(C=0),T) 1400(D), 1583(G), 2415(D″ + D), 2800(2D), 3190(2G), 1049(d(CO)), 1100(DP), 1294(A), 1327(A), 1747, 2090(d(CH)), 2701(d(CH)), 2949(d(CH))	λ = 532 nm, RT λ = 473 nm, RT λ = 355 nm, RT Red shift of frequencies for guanine upon cooling [20] λ = 532 nm, 30 K Red shift of frequencies for Adenine upon cooling [20]; Red shift of band d(CO); λ = 355 nm, 26 K

*Molecular groups of DNA are labeled in the following way. A, Gu, C, and T are the nucleobases adenine, guanine, cytosine, and thymine, respectively; d is deoxyribose; DP is phosphodiester bond

Table 17.4 Characteristic molecular vibrations, observed in the Raman spectra of complexes oligonucleotide/MWCNT at laser excitation with wavelengths $\lambda = 532$ nm and RT

Sample	Bands, cm^{-1}	Assignment	t12.1
Oligonucleotide-	1340(D), 1572(G);	MWCNTs	t12.2
encased MWCNTs inside SA-micelle	1605(A)	adenine	t12.3
LB-film from	1340(D), 1571(G);	MWCNTs	t12.4
oligonucleotide-encased MWCNTs and SA	1605(A)	adenine	t12.5

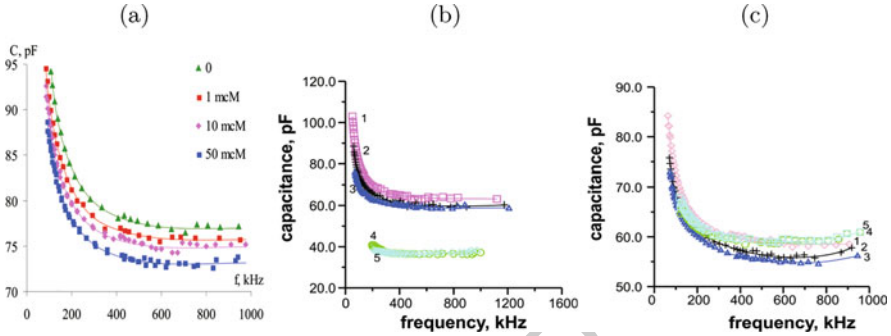

Fig. 17.1 Bode capacity plots for DNA-sensors. (**a**) DNA-sensor K11 with homoduplexes between probe DNA KRAS*m* and recognized colorectal cancer tumor DNA after 30 min exposure of thymoquinone at different concentrations. (**b**–**c**) DNA-sensor R18 (**b**) and F32 (**c**): 1 – pure sensor, 2 – sensor with electrodes coated by LB-film from nanocyclic organometallic complexes, 3 – sensor with electrodes coated by LB-film from DNA probe allocated on MWCNTs decorated by metal atoms, 4 – deposition of 1.3 ng/μL DNA_{pv1} (**b**) or 0.7 ng/μL DNA_{h1} (**c**), 5 – deposition of 2.6 ng/μL DNA_{pv1} (**b**) or 1.4 ng/μL DNA_{h1} (**c**)

and probe ss-DNAs, as in the case of ds-DNA isolated from blood of patients with parvovirus infection (ds-DNA_{pv1}) (Fig. 17.1b). The hybridization of DNA probe molecule with target DNA molecule that is ss-DNA released at denaturation of the original ds-DNA proceeds on the sensor surface. The complementary target ss-DNA bound with the ss-DNA probe $B19VR4$ of sensor penetrates in the sensitive layer of transducer through the nanocavities of LB-DTP-film into nanopores of AOA with subsequent binding of MWCNTs ends and a shielding effect emerges. In the individual case the capacitance decrease has been registered for DNA sample with parvovirus only at DNA concentration 3 ng/μL. The decrease of sensor capacitance indicates the complementary interaction of revers-primer probe DNA with viral DNA from patient's DNA samples.

A target ss-DNA which is noncomplementary to the ss-DNA probe reacts very quickly with another complementary ssDNA forming the original target ds-DNA. Since a diameter of this ds-DNA is larger than the nanocavities, the shielding effect is absent and a capacitance of sensor increases (Fig. 17.1c).

The dielectric loss is measured as the inverse capacity C^{-1} of sensor. Spectra of Cole-Cole plots are dependencies of the dielectric losses on signal power W. These dependencies correspond to the dependencies of dielectric loss constant

on the real part of complex dielectric permeability (dielectric dispersion). As one can see in Fig. 17.2, the Cole-Cole plots of pure sensors without sensitive coating are characterized by the presence of three Cole-Cole plots with characteristic frequencies $\lambda_0, \lambda_1, \lambda_2$ of dipole relaxation in the range in signal power value W from 2 to 25 V*V. In addition to a capacitance of electrically charged Helmholtz double layer, there is a Warburg impedance element of diffusion layer at signal power more than 40 V*V.

Deposition of sensor coating leads to appearing of additional frequencies λ_p and λ_{ON} of relaxation oscillations of dipoles in the LB-DTP-film and oligonucleotide-MWCNT-LB-film, as Fig. 17.2 demonstrates. In Fig. 17.2c, d the data of electrochemical response of the sensors on hybridization of probe oligonucleotides with DNA isolated from the blood of patient with parvovirus infection are presented. As one can see, hybridization of oligonucleotide with complementary viral DNA results in appearing additional frequency λ_{DNA} of dipole relaxation at signal power 17–19 V*V. For revers primer $B19VR4$ along with the appearing the Cole–Cole plots λ_{DNA} dielectric losses increase (screening effect).

The characteristic Cole–Cole plots λ_{DNA} are absent at non-complementary hybridization between target DNA of all samples obtained from healthy donors and both the DNA probes $B19VR4$ and $B19VF4$ (see Fig. 17.2a, b). Since dielectric losses decrease and accordingly the screening effect is absent an increase of capacity emerges after the noncomplementary hybridization.

17.4 Discussion and Conclusion

The Raman and impedance spectroscopic assays demonstrate that charge CNT-carriers are confined on CNT-surface. Quinone, intercalating into ds-DNA helix, keeps sterically its nucleosides away from CNT-surface. Since the CNT charge carriers can not be transported (localized) on the remote impurity defects, a number of free CNT charge carriers increases by the number of charge carriers localized before. Meanwhile $\pi - \pi$-bonds between nucleosides and CNT-surface break. Due to an attenuation of $\pi - \pi$-interactions conformational mobility of DNA increases and a conformation of DNA molecules attaching to CNT-ends that MWCNTs linked with DNA form a network is an energy-efficient DNA configuration. Hopping conduction of DNA appears after doping in the sites of contact between the DNA molecules and the end groups. The number of contacts increases with thymoquinone concentration (see Fig. 17.1a). Now, a transport of electrical charge occurs along two systems. Since both of systems are high-conductivity ones, screening of near-electrode Helmholtz layer by the DNA–CNT network is more effective than by the MWCNT LB-bundles. The native-DNA sequencing performed and presented in the paper is based on this double shielding of external electrical fields. The DNA doped by CNT-ends on sensor surface results from conformal wandering of complementary ss-DNA which penetrates through nanocavities in the LB-film of nanocyclic compound Fe(II)DTP in the nanoporous AOA.

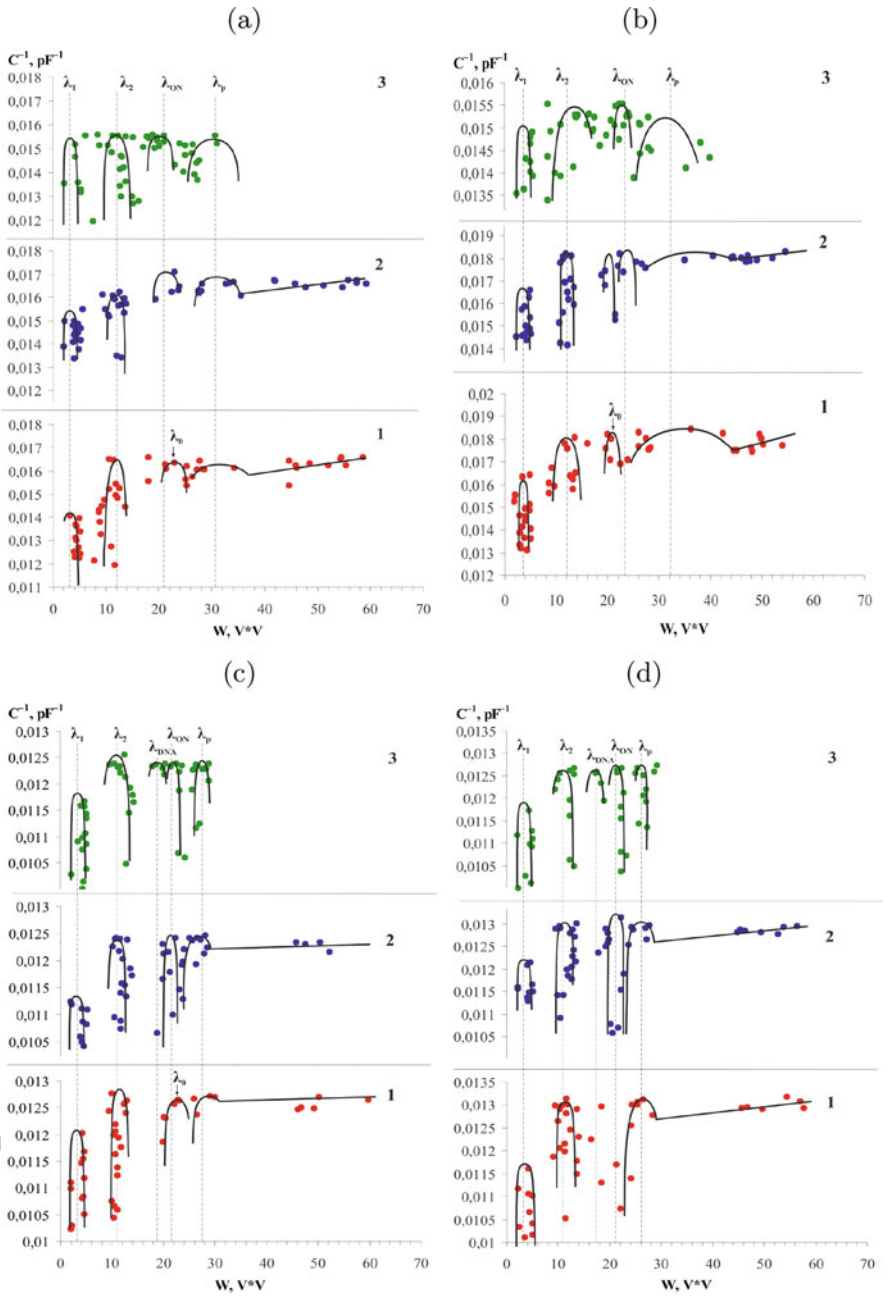

Fig. 17.2 Dielectric spectra with Cole–Cole plots for sensors with LB-DTP-film (curve 1), coated with LB-CNT-film with oligonucleotide before (curve 2) and after hybridization with DNA (curve 3). (**a**, **b**) DNA isolated from healthy donors: control DNA_{h2} (**a**) on sensor R0 and DNA_{h3} (**b**) on sensor F24; deposition of 0.7 ng/μL. (**c**, **d**) DNA isolated from the blood of patients with parvovirus infection, deposition of 1.0 ng/μL DNA_{pv2} on sensor R4 (**c**) and sensor F14. Characteristic maxima of the plots are λ_0, λ_1, λ_2 for AOA; λ_p for LB-DTP-film, λ_{ON} for DNA probe, λ_{DNA} for target DNA

So, the proposed dielectric-spectroscopy method allows to detect the presence or absence of target viral infection in DNA samples and can be used as an alternative laboratory diagnostic method.

References

1. Grushevskaya HV et al (2019) Single-molecule EIS-sequencing of DNA on composite nanoporous structures: advances and perspectives. Sci Innov 4(194):23 (in Russian)
2. Labunov V, Shulitski B, Prudnikava A, Shaman YP, Basaev AS (2010) Composite nanostructure of vertically aligned carbon nanotube array and planar graphite layer obtained by the injection CVD method. Quantum Electron Optoelectron 13:137
3. Kel'in A, Kulinkovich O (1995) A new synthetic approach to the conjugated five numbered heterocycles with long-chain substituents. Folia Pharm Univ Carol (supplementum) 18:96
4. Grushevskaya HV, Krylova NG, Lipnevich IV, Babenka AS, Egorova VP, Chakukov RF (2018) CNT-based label-free electrochemical sensing of native DNA with allele single nucleotide polymorphism. Semiconductors 52(14):1836
5. Grushevskaya HV, Lipnevich IV, Orekhovskaya TI (2013) Coordination interaction between rare earth and/or transition metal centers and thiophene series oligomer derivatives in ultrathin Langmuir–Blodgett films. J Mod Phys 4:7
6. Egorov AS, Krylova HV, Lipnevich IV, Shulitsky BG, Baran LV, Gusakova SV, Govorov MI (2012) Structure of modified multi-walled carbon nanotube clusters on conducting organometallic Langmuir–Blodgett films. J Nonlin Phenom Complex Syst 15:121
7. Repetsky SP, Vyshyvana IG, Nakazawa Y, Kruchinin SP, Bellucci S (2019) Electron transport in carbon nanotubes with adsorbed chromium impurities. Materials 12:524
8. Repetsky SP, Vyshyvana IG, Kruchinin SP, Bellucci S (2018) Influence of the ordering of impurities on the appearance of an energy gap and on the electrical conductance of graphene. Sci Rep 8:9123
9. Filikhin I, Peterson TH, Vlahovic B, Kruchinin SP, Kuzmichev YuB, Mitic V (2019) Electron transfer from the barrier in InAs/GaAs quantum dot-well structure. Phys E Low-dimensional Syst Nanostruct 114:113629
10. Ermakov V, Kruchinin S, Pruschke T, Freericks J (2015) Thermoelectricity in tunneling nanostructures. Phys Rev B 92:115531
11. Kruchinin S, Pruschke T (2014) Thermopower for a molecule with vibrational degrees of freedom. Phys Lett A 378:157–161
12. Egorov AS, Egorova VP, Grushevskaya GV, Krylova NG, Lipnevich IV, Orekhovskaya TI, Shulitsky BG (2016) CNTenhanced Raman spectroscopy and its application: DNA detection and cell visualization. Lett Appl NanoBioSci 5:343
13. Tsai YT, Choi CH, Gao N, Yang EH (2011) Tunable wetting mechanism of polypyrrole surfaces and low-voltage droplet manipulation via redox. Langmuir 27:4249
14. Jeon SH, Lee HJ, Bae K, Yoon K-A, Lee ES, Cho Y (2016) Efficient capture and isolation of tumor-related circulating cell-free DNA from cancer patients using electroactive conducting polymer nanowire platforms. Theranostics 6:828
15. Cooper DR et al (2012) Experimental review of graphene. ISRN Condens Matter Phys 2012:501686
16. Potcoava MC, Futia GL, Aughenbaugh J, Schlaepfer IR, Gibson EA (2014) Raman and coherent anti-Stokes Raman scattering microscopy studies of changes in lipid content and composition in hormone-treated breast and prostate cancer cells. J Biomed Opt 19(11):111605
17. Deepika, Hait SK, Chen Y (2014) Optimization of milling parameters on the synthesis of stearic acid coated $CaCO_3$ nanoparticles. J Coat Technol Res 11(2):273

18. Grushevskaya HV, Krylova NG, Lipnevich IV, Egorova VP, Babenka AS (2018) Single nucleotide polymorphism genotyping using DNA sequencing on multiwalled carbon nanotubes monolayer by CNT-plasmon resonance. Int J Mod Phys B 32(17):1840033
19. Prescott B, Steinmetz W, Thomas GJ Jr (1984) Characterization of DNA structures by laser Raman spectroscopy. Biopolymers 23(2):235
20. Anokhin AS, Gorelik VS, Dovbeshko GI, Pyatyshev AYu, Yuzyuk YuI (2015) Difference Raman spectroscopy of DNA molecules. J Phys Conf Ser 584:012022
21. Zhizina GP, Oleinik EF (1972) Infrared spectroscopy of nucleic acids. Russ Chem Rev 41(3):474
22. Grushevskaya HV, Krylova NG, Lipnevich IV, Orekhovskaja TI, Egorova VP, Shulitski BG (2016) Enhancement of Raman light scattering in dye-labeled cell membrane on metal-containing conducting polymer film. Int J Mod Phys B 30:1642018
23. Gutierrez PL (2000) The metabolism of quinone-containing alkylating agents: free radical production and measurement. Front Biosci 5:d629
24. Esteves-Souza A et al (2007) Cytotoxic and DNA-topoisomerase effects of lapachol amine derivatives and interactions with DNA. Braz J Med Biol Res 40:1399
25. Hasinoff BB et al (2006) Structure-activity study of the interaction of bioreductive benzoquinone alkylating agents with DNA topoisomerase II. Cancer Chemother Pharmacol 57:221
26. Martinez R, Chacon-Garcia L (2005) The search of DNA-intercalators as antitumoral drugs: what it worked and what did not work. Curr Med Chem 12:127
27. Grushevskaya HV, Krylova NG (2018) Carbon nanotubes as a high-performance platform for target delivery of anticancer quinones. Curr Pharm Des 24(43):5207